low-size Ru particles from construction of 3D RGO/CNT carrier for boosting oxygen reduction reaction

Haonan Shen [a], Tongtong Lian [a], Yide Hao [a], Yongxiang Wang [a], Zongyu Zhang [a], Yanchao Jin [c], Jiangshan Gao [a, *], Yan He [a, b, *]

[a] College of Electromechanical Engineering, Qingdao University of Science and Technology, Shandong Engineering Laboratory for Preparation and Application of High-Performance Carbon Materials, Qingdao 266061, P. R. China

[b] Qingdao University, Qingdao 266061, P. R. China.

[C] Doright Co., Ltd.

*Email: gaojs@qust.edu.cn, heyan@qust.edu.cn

Supporting Information

1 Experimental Section

1.1 Chemicals

Ru (III) chloride hydrate ($RuCl_3 \cdot xH_2O$), graphene oxide (GO), carbon nanotubes (CNTs), platinum-carbon catalyst (Pt/C, 20 wt%), Nafion solution ($C_9HF_{17}O_5S$, 5 wt%), potassium hydroxide (KOH), and ethanol absolute (CH_3CH_2OH) were purchased from Aladdin Reagent Co., Ltd. and used as received without further purification.

1.2 Synthesis of Ru@RGO/CNT

A mixture containing 10 mg of graphene oxide and 20 mg of carbon nanotubes was precisely weighed and transferred into a 30 mL capped quartz crucible. To this, 20 mL of ethylene glycol was added, and the suspension was ultrasonicated for 4 hours to ensure homogeneous dispersion. During ultrasonication, 1.5 mL of a pre-prepared 10 mg mL^{-1} Ru chloride aqueous solution was introduced dropwise, followed by an additional hour of ultrasonication. After cooling to ambient temperature, the solution was subjected to microwave irradiation using a reactor programmed for four cycles of 50 seconds active heating and 10 seconds cooling intervals at full power. Post-reaction, the cooled mixture was centrifuged at 10,000 rpm for 3 minutes per cycle and repeatedly washed with deionized water to eliminate residual ethylene glycol. The final product was vacuum-dried at 70°C.

To evaluate the influence of the graphene oxide-to-carbon nanotube mass ratio on structural and catalytic properties, samples were synthesized with varying GO/CNT ratios while maintaining identical processing conditions. These were designated as Ru@RGO/CNT-3/0, Ru@RGO/CNT-2/1, Ru@RGO/CNT-1/2, and Ru@RGO/CNT-0/3. Parallel experiments explored the effect of Ru precursor loading by adjusting the volume of $RuCl_3$ aqueous solution added. Corresponding products were labeled Ru@RGO/CNT-1, Ru@RGO/CNT-2, Ru@RGO/CNT-3, and Ru@RGO/CNT-4 to reflect incremental increases in $RuCl_3$ volume.

1.3 Materials characterizations

In this study, the surface morphology of the catalysts was characterized using a SU8010 scanning electron microscope (SEM). The microstructure, high-resolution transmission electron microscopy (HRTEM) images, and selected-area electron diffraction (SAED) patterns were obtained with an H-8100 transmission electron microscope (TEM) equipped with energy-dispersive X-ray spectroscopy (EDX). The crystallographic phases of the catalysts were analyzed using a MiniFlex600 X-ray

diffractometer (XRD) with a scanning range of 5° to 90°. The defect structures of the samples were investigated via an In Via Reflex Raman spectrometer. Elemental composition and valence states were determined using an AXIS SUPRA$^+$ X-ray photoelectron spectrometer (XPS).

1.4 Electrochemical Measurements

All tests were conducted at 25°C using a three-electrode electrochemical workstation (CHI 760E, Shanghai, China). A 0.1 M KOH solution was used as the electrolyte, with a rotating ring-disk electrode (RRDE, 5 mm diameter) serving as the working electrode, a platinum wire as the counter electrode, and an Ag/AgCl electrode as the reference electrode. The catalyst ink was prepared by dispersing 5 mg of the catalyst in 490 μL of ethanol and 10 μL of Nafion solution through ultrasonication. The 5 μL well-dispersed ink was drop-cast onto the RRDE and dried at room temperature to obtain a catalyst-modified working electrode (catalyst loading: 0.255 mg cm^{-2}). In this study, the reversible hydrogen electrode (RHE) was used as the reference for potential calibration. The relationship between the potential and the Ag/AgCl reference electrode is shown in Equation (1), where "E" represents the potential measured against the Ag/AgCl reference electrode, and $E_{\mathrm{Ag/AgCl}}$(vs. SHE) is the reference potential of the Ag/AgCl electrode. In this experiment, the potential of the Ag/AgCl reference electrode was 0.1989 V. During testing, all potentials were calibrated to the RHE scale, and 95% iR compensation was applied to all parameters.

$$E_{RHE} = E + E_{Ag/AgCl}(vs.RHE) + 0.0591 \bullet pH \quad (1)$$

Cyclic voltammograms (CV) were recorded in O_2- and N_2-saturated electrolytes at a constant scan rate of 50 mV s^{-1}. Linear sweep voltammetry (LSV) was conducted at a scan rate of 10 mV s^{-1} by varying the rotation speed of the rotating ring-disk electrode (RRDE) to 400, 900, 1600, and 2500 rpm. The i-t chronoamperometric curves were recorded at a rotation speed of 1600 rpm to evaluate the catalyst's stability and methanol tolerance. Additionally, the electron transfer number (n) for the oxygen reduction reaction (ORR) was calculated using the Koutecky-Levich (K-L) equation, as detailed below.

$$\frac{1}{J} = \frac{1}{J_L} + \frac{1}{J_K} = \frac{1}{B\omega^{1/2}} + \frac{1}{J_K} \quad (2)$$

$$B = 0.62nFC_0\upsilon^{-1/6}D_0^{2/3} \quad (3)$$

In the equations, j represents the total measured current density (A cm^{-2}), j_L is the diffusion-limited current density related to the oxygen diffusion rate, j_K is the kinetic current density associated with the reaction rate constant, and ω denotes the angular velocity of the rotating electrode (rad s^{-1}). Additionally, the parameters are defined as follows:

- n: the number of electrons transferred during the reaction
- F: Faraday's constant (96485 C mol^{-1})
- C_O: the oxygen concentration in the solution (in 0.1 M KOH, C_O=1.2×10^{-6} mol cm^{-3})
- D_O: the diffusion coefficient of oxygen (in 0.1 M KOH, D_O=1.9×10^{-5} $cm^2 \cdot s^{-1}$),
- ν: the kinematic viscosity of the electrolyte (in 0.1 M KOH, ν=0.01 $cm^2 \cdot s^{-1}$).

The methanol tolerance test is conducted under a constant voltage, where the catalyst operates for approximately 200 seconds. After adding 3 M methanol to the electrolyte, the methanol tolerance is evaluated by analyzing the changes in the chronoamperometric (time-current) curve. The stability test is performed under a constant voltage in an O_2-saturated 0.1 M KOH solution. The stability of the ORR catalyst is characterized by monitoring the current variation over time during its long-term operation.

The hydrogen peroxide yield ($\%HO_2^-$) and electron transfer number (n) during the oxygen reduction reaction were quantitatively determined using the following equations:

$$\%HO_2^- = 200 \times \frac{I_r/n}{I_d + I_r/N} \quad (4)$$

$$n = 4 \times \frac{I_d}{I_d + I_r/N} \quad (5)$$

where N = 0.42 is the experimentally determined collection efficiency of the RRDE system, I_r and I_d represent the ring and disk currents (mA), respectively.

2 Results and discussion

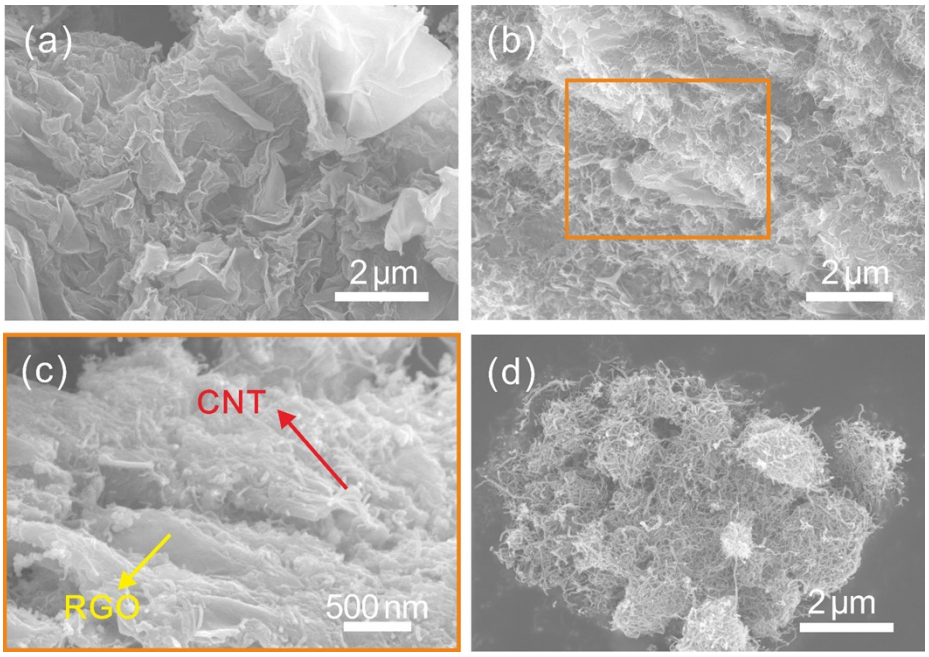

Figure S1. (a) Ru@RGO/CNT-3/0, (b) Ru@RGO/CNT-2/1, (c) Ru@RGO/CNT-2/1, (d) Ru@RGO/CNT-0/3 SEM images.

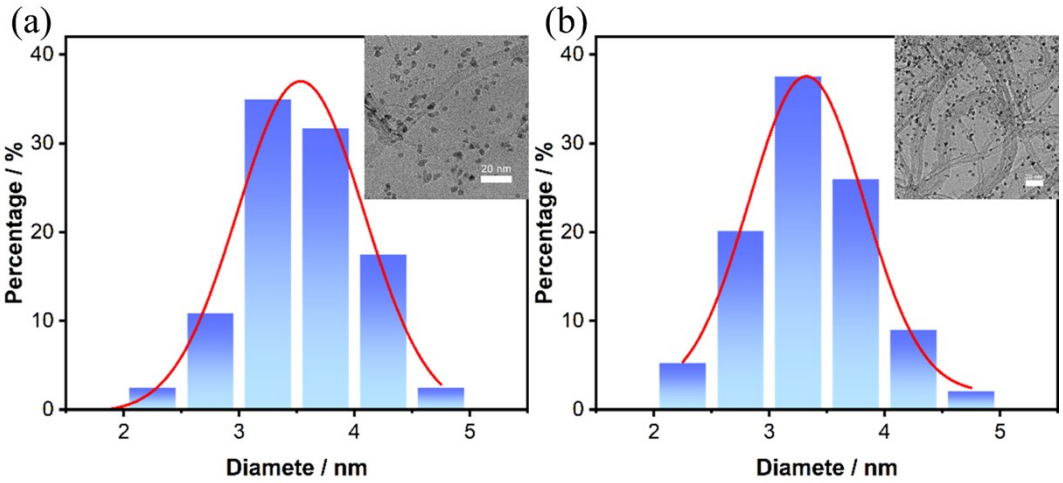

Figure S2. (a) Particle size distribution diagram and TEM, (b) post-test TEM images together with an updated particle-size distribution of Ru@RGO/CNT-1/2.

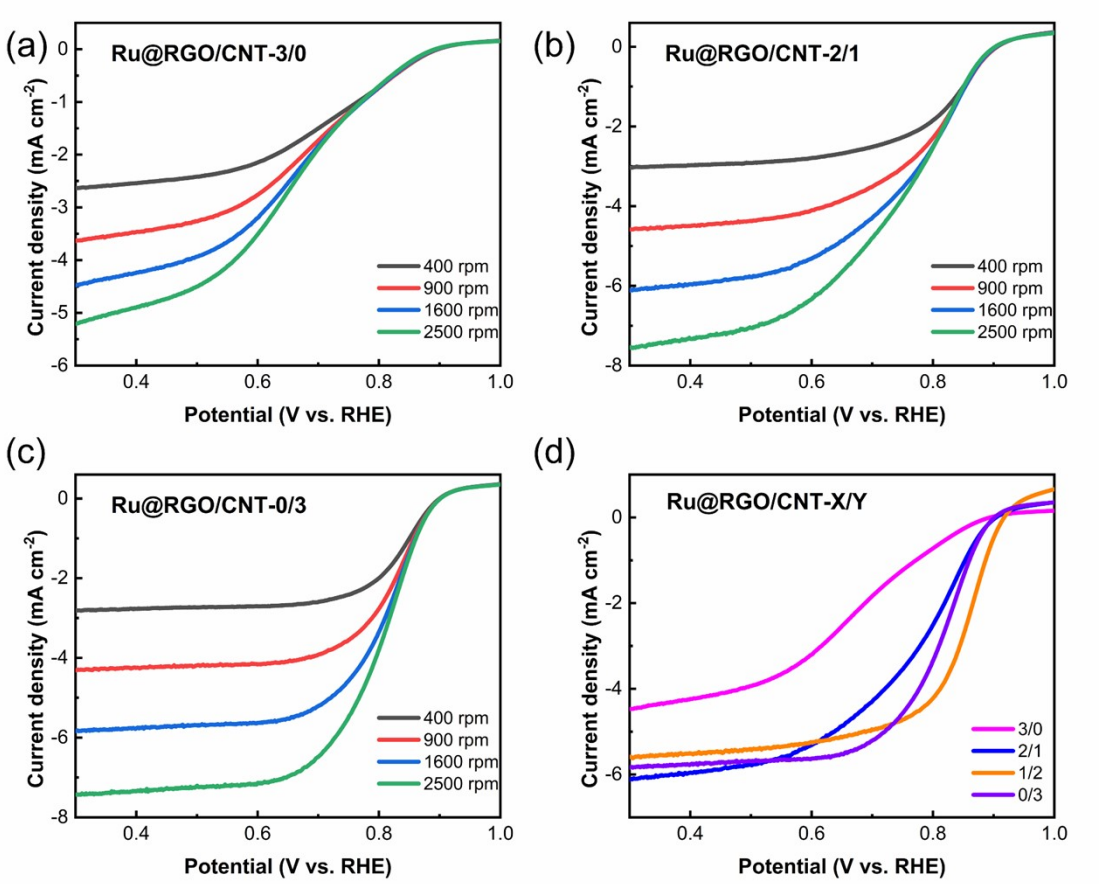

Figure S3. (a-c) LSV curves of Ru@RGO/CNT-3/0, Ru@RGO/CNT-2/1, and Ru@RGO/CNT-0/3 catalysts. (d) LSV curves of Ru@RGO/CNT-X/Y catalysts at a rotation speed of 1600 rpm.

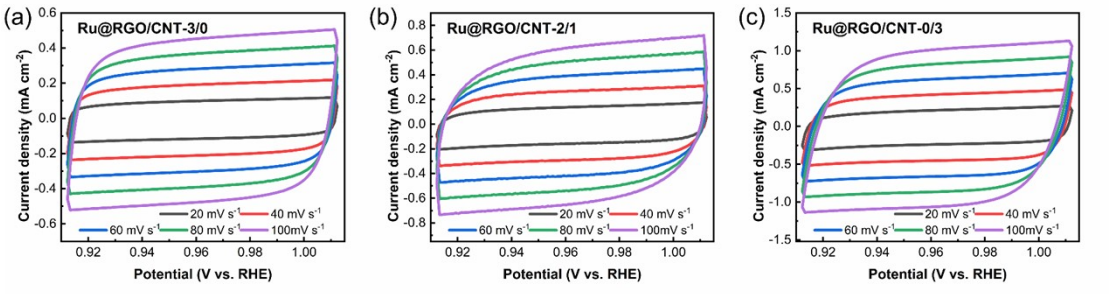

Figure S4. (a-c) CV curves of Ru@RGO/CNT-3/0, Ru@RGO/CNT-2/1, and Ru@RGO/CNT-0/3 at scan rates ranging from 20 to 100 mV s^{-1}.

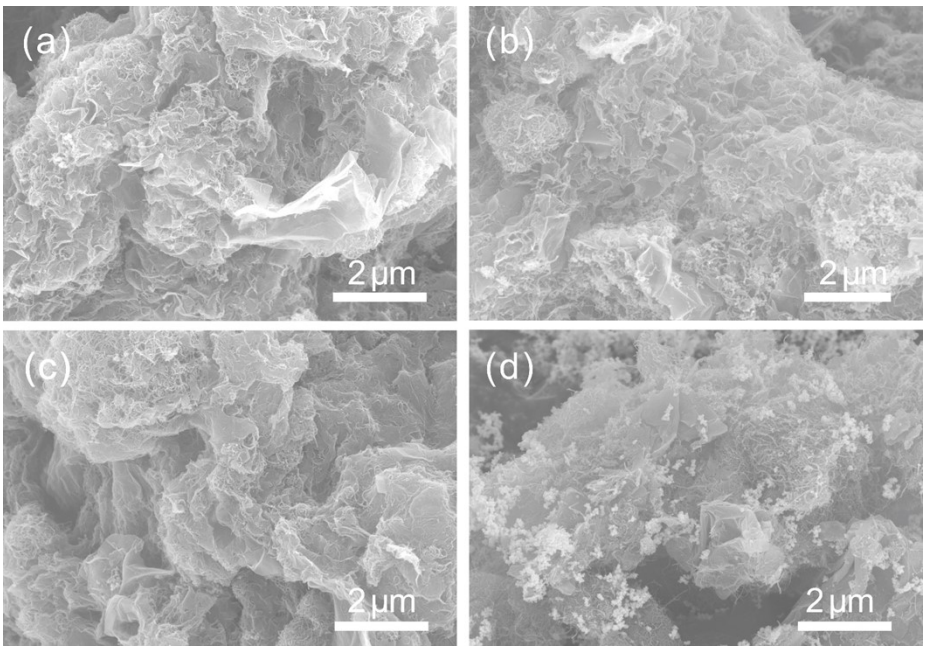

Figure S5. (a) SEM image of Ru@RGO/CNT-1, (b) SEM image of Ru@RGO/CNT-2, (c) SEM image of Ru@RGO/CNT-3, (d) SEM image of Ru@RGO/CNT-4.

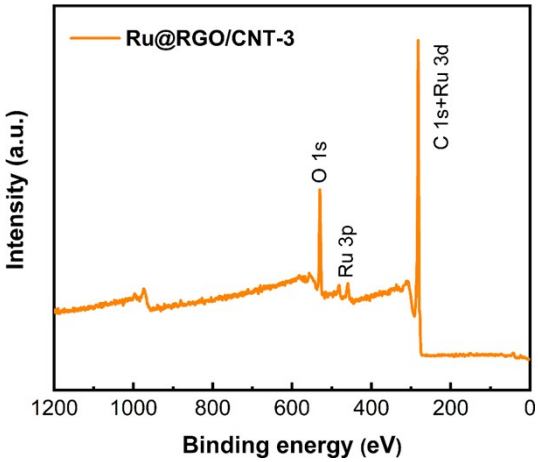

Figure S6. XPS survey spectrum of Ru@RGO/CNT-3.

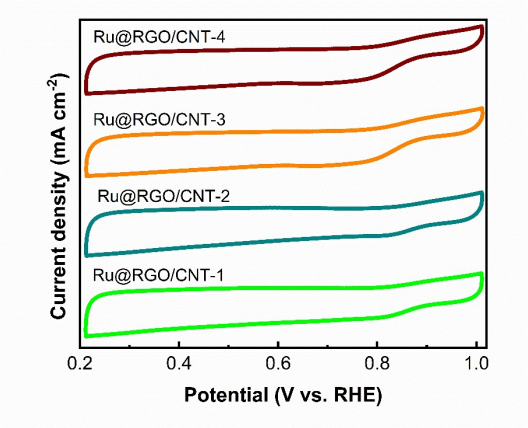

Figure S7. CV curves of Ru@RGO/CNT-X

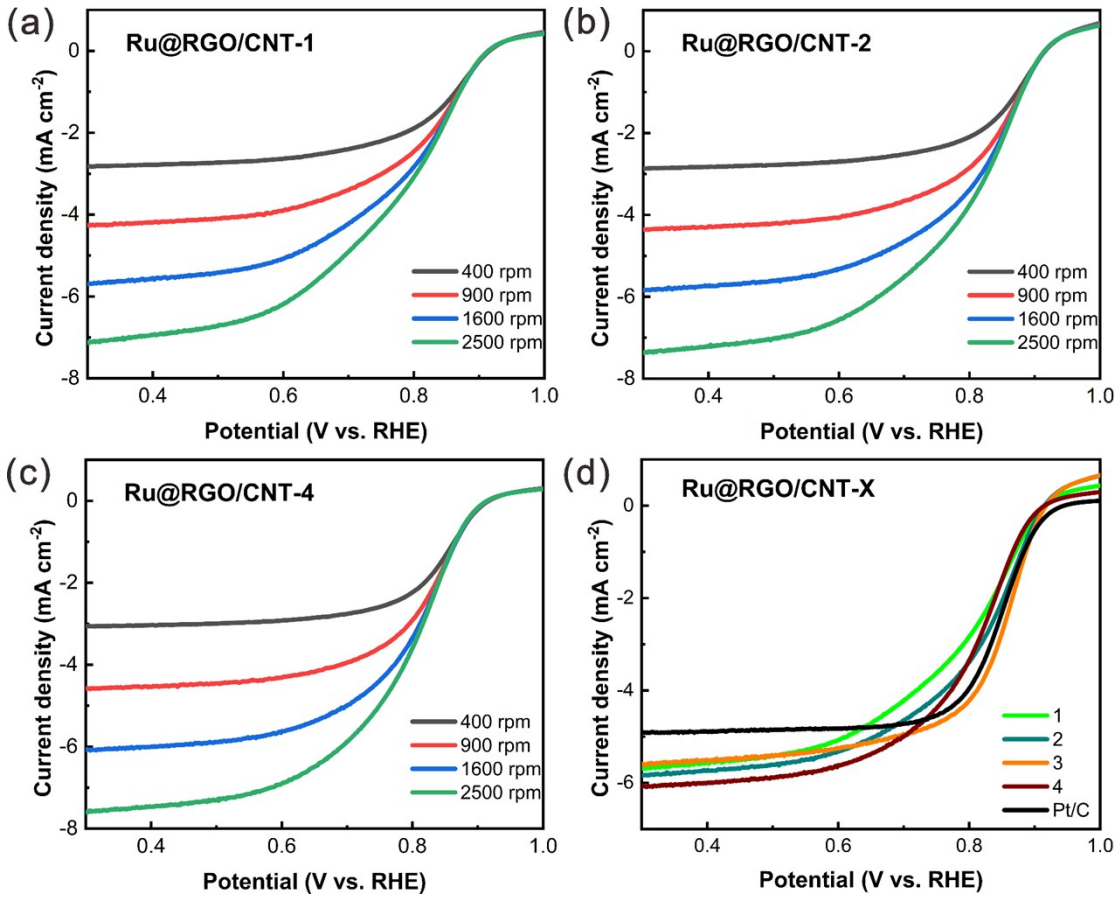

Figure S8. (a-c) LSV curves of Ru@RGO/CNT-1, Ru@RGO/CNT-2, and Ru@RGO/CNT-4 catalysts, (d) the LSV curves at a rotating speed of 1600 rpm

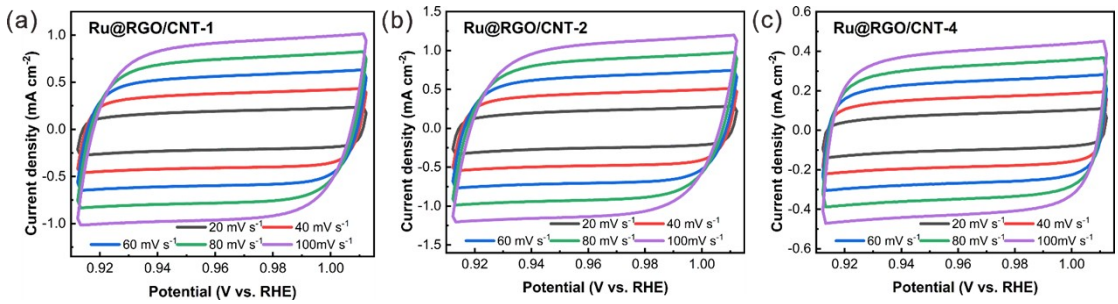

Figure S9. (a-c) CV curves of Ru@RGO/CNT-1, Ru@RGO/CNT-2, and Ru@RGO/CNT-4 at scan rates ranging from 20 to 100 mV s^{-1}.

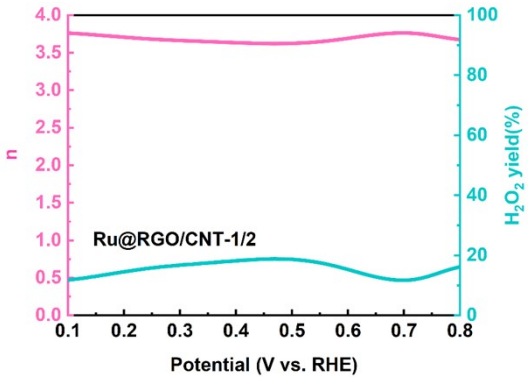

Figure S10. n and H_2O_2 yield of Ru@RGO/CNT-1/2

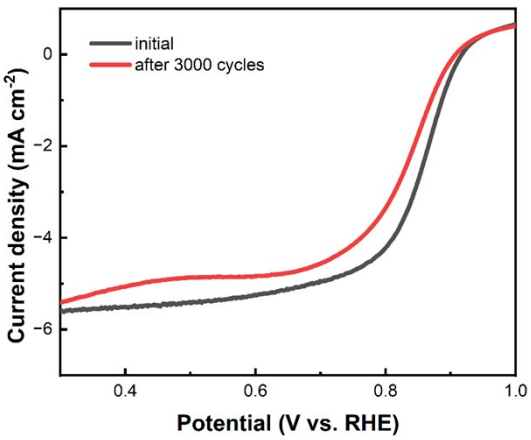

Figure S11. LSV curves of Ru@RGO/CNT-3 before and after 3000 CV cycles.

Table S1. Comparative ORR Electrochemical Performance of Ru-based Catalyst with Recently Reported Results

Catalysts	**$E_{1/2}$(V)**	**Tafel slope (mV dec^{-1})**	**Ref**
RuBCN	0.76	38.9	[1]
Ru/HNCS	0.72	107	[2]
Ru/N-G-500	0.847	52.6	[3]
Ru-Co_3O_4	0.81	-	[4]
$RuSe_2$/C	0.77	-	[5]
Co-Ru/NCN	0.81	64	[6]
Ru@RGO/CNT	0.85	53.14	**This Work**

References

[1] Sun X, Wu B, Li B, Zhao J, Li S, Zheng M, et al. Strong metal-support interactions for high sintering resistance of Ru-based catalysts toward the HER and ORR. Chem Commun 2023;59:10291–4. https://doi.org/10.1039/D3CC02529B.

[2] Jiang A, Wang Z, Li Q, Dong M. An efficient ruthenium-based dual-electrocatalyst towards hydrogen evolution and oxygen reduction reactions. Materials Today Physics 2021;16:100300. https://doi.org/10.1016/j.mtphys.2020.100300.

[3] Liu S, Dai L, Qu Y, Qiu Y, Fan J, Li X, et al. Crystalline/amorphous hetero-phase Ru nanoclusters for efficient electrocatalytic oxygen reduction and hydrogen evolution. Mater Chem Front 2021;5:6648–58. https://doi.org/10.1039/D1QM00812A.

[4] Hu D, Wang R, Du P, Li G, Wang Y, Fan D, et al. Electrospinning Ru doped Co3O4 porous nanofibers as promising bifunctional catalysts for oxygen evolution and oxygen reduction reactions. Ceramics International 2022;48:6549–55. https://doi.org/10.1016/j.ceramint.2021.11.202.

[5] Gong Q, Hu P, Yang W, Zhang T, Liu J, Li H, et al. Microwave-Assisted Preparation of the Cubic $RuSe_2$ /C Catalyst for Fuel Cell Applications. ACS Appl Energy Mater 2022;5:13166–75. https://doi.org/10.1021/acsaem.1c03990.

[6] Wang H, Yang P, Sun X, Xiao W, Wang X, Tian M, et al. Co-Ru alloy nanoparticles decorated onto two-dimensional nitrogen doped carbon nanosheets towards hydrogen/oxygen evolution reaction and oxygen reduction reaction. Journal of Energy Chemistry 2023;87:286–94. https://doi.org/10.1016/j.jechem.2023.08.039.